Landslides (2011) 8:33–48
DOI 10.1007/s10346-010-0222-z
Received: 5 January 2009
Accepted: 11 May 2010
Published online: 15 June 2010


Simon K. Allen · Simon C. Cox · Ian F. Owens

# Rock avalanches and other landslides in the central Southern Alps of New Zealand: a regional study considering possible climate change impacts

**Abstract** Slope instabilities in the central Southern Alps, New Zealand, are assessed in relation to their geological and topographic distribution, with emphasis given to the spatial distribution of the most recent failures relative to zones of possible permafrost degradation and glacial recession. Five hundred nine mostly late-Pleistocene- to Holocene-aged landslides have been identified, affecting 2% of the study area. Rock avalanches were distinguished in the dataset, being the dominant failure type from Alpine slopes about and east of the Main Divide of the Alps, while other landslide types occur more frequently at lower elevations and from schist slopes closer to the Alpine Fault. The pre-1950 landslide record is incomplete, but mapped failures have prevailed from slopes facing west–northwest, suggesting a structural control on slope failure distribution. Twenty rock avalanches and large rockfalls are known to have fallen since 1950, predominating from extremely steep east–southeast facing slopes, mostly from the hanging wall of the Main Divide Fault Zone. Nineteen occurred within 300 vertical metres above or below glacial ice; 13 have source areas within 300 vertical metres of the estimated lower permafrost boundary, where degrading permafrost is expected. The prevalence of recent failures occurring from glacier-proximal slopes and from slopes near the lower permafrost limit is demonstrably higher than from other slopes about the Main Divide. Many recent failures have been smaller than those recorded pre-1950, and the influence of warming may be ephemeral and difficult to demonstrate relative to simultaneous effects of weather, erosion, seismicity, and uplift along an active plate margin.

**Keywords** Landslide inventory · Rock avalanche · Glacial change · Permafrost · Southern Alps · New Zealand

## Introduction

Landslides are a major process in hillslope evolution (Densmore and Hovius 2000; Korup et al. 2005), impact upon rivers (Korup 2002; Korup 2005a) and glacial systems (Hewitt et al. 2008; Shulmeister et al. 2009) and are a serious hazard in many regions of the world (Nadim et al. 2006). In glaciated Alpine terrain, landslides often involve large volumes and travel distances, owing to high local relief, enhanced travel over ice or snow surfaces, flow transformations and chain-reaction events (e.g. Evans and Clague 1988; Haeberli et al. 2004). In addition, the hazard associated with slope instabilities in glacial environments is highly dynamic because recent atmospheric warming is rapidly altering glacial landscapes and may be shifting zones of instability and initiation (Kääb et al. 2005; Geertsema et al. 2006). Landslides and other gravitational mass wasting play a significant role in the erosion of New Zealand's Southern Alps (Hovius et al. 1997; Korup et al. 2004). This mountain chain is being actively formed by the convergence of two tectonic plates. Stress-release fracturing and dilation of mountain rock masses occurs during uplift and exhumation. Over time, effects such as rock-mass dilation, ice wedging, glacier and snow level recession, and the reduction in ice-binding of rock masses combine to lower their resistance to failure (Wegmann et al. 1998; Davies et al. 2001; Gruber and Haeberli 2007). Major earthquakes and storms have triggered slope failures (e.g. Whitehouse and Griffiths 1983; Hancox et al. 2003), but numerous spontaneous events have also occurred (McSaveney 2002; Cox and Allen 2009).

Recent completion of a digital geological map and geographic information system (GIS) dataset (Cox and Barrell 2007) creates an opportunity to better study landslide distribution in the Southern Alps and to discuss possible impacts of glacier recession and permafrost warming in the region. The dataset provides an inventory of over 500 landslides in the central South Island, for which related geology and topography can be explored in a GIS environment. This study begins with a description of the physical setting, before providing an overview of the regional topography characterising the central Southern Alps. The main objective of this paper is to examine the distribution of landslides from this past century in relation to local geology and topography, but within the context of a much longer record of landslide activity. If effects of twentieth century climate change are evident within this tectonically active mountain belt, a significant correlation would be expected between the occurrence of recent slope failures and the extent of glacial or periglacial zones.

## Background

Slope stability is primarily governed by rock-mass strength, slope angle and slope height, which vary in different geological and geomechanical settings. In high-mountain environments, geological hazards are increasingly being studied in relation to possible interactions with changing glacial and permafrost conditions (e.g. Evans and Clague 1988; Harris 2005; Deline 2009; Huggel 2009). Bedrock walls in glacial environments are typically steep, with erosion of their lower flanks potentially exacerbated by glacial plucking (Ballantyne 2002). Subsequent retreat of glacial ice can induce changes in the stress field of the surrounding rock walls and expose previously insulated surfaces to altered mechanical and thermal erosion (Haeberli et al. 1997; Wegmann et al. 1998). The influence of permafrost degradation within steep rock walls is a relatively new field of research stemming from initial theoretical discussions linking atmospheric warming, glacier recession, permafrost degradation and slope instability (Haeberli et al. 1997; Harris and Vonder Mühll 2001). Laboratory studies have since demonstrated that the shear strength of an ice-bonded rock discontinuity significantly reduces with warming, revealing a minimum factor of safety at temperatures between −1.5°C and 0°C, where a discontinuity may be less stable than when in a completely thawed state (Davies et al. 2001).

Other factors including ice segregation and volume expansion are likely to predispose a rock discontinuity to subsequent failure upon warming (Gruber and Haeberli 2007), and meltwater or ground-water flow into a previously frozen fracture may cause elevated water pressure and reduced frictional strength (Harris 2005). An absence of snow, ice or debris cover on steep slopes means that sub-surface temperatures and related bedrock stability can respond rapidly (within one season to several years) to atmospheric warming. This was demonstrated during the extremely warm European summer of 2003, when numerous rockfalls were likely associated with extreme heat fluxes in the active layer of the alpine permafrost, with massive ice observed in some detachment zones (Gruber et al. 2004). Deeper warming of Alpine permafrost is delayed in the order of decades to centuries, but warming of 0.5°C to 0.8°C in the upper decametres has been observed over the past century in Europe (Harris et al. 2003) and has been linked to rock avalanches from deeper detachment surfaces occurring primarily in estimated areas of warm or degrading permafrost warmer than –1.5°C; Dramis et al. 1995; Bottino et al. 2002; Noetzli et al. 2003). Within landslide-inventory studies, slope-failure susceptibility has been explored on the basis of individual or combined causative factors such as slope, lithology, geological structure, slope morphology and anthropogenic activities (e.g. Hermanns and Strecker 1999; Pande et al. 2002; Pike et al. 2003). Relating landslide susceptibility to permafrost and glacial factors is faced with greater uncertainty because these factors are often difficult to observe or measure and change rapidly over time, but some important linkages have been proposed from a small inventory of recent landslides in the European Alps (Noetzli et al. 2003), and further insights have been gained from detailed case studies (e.g. Gruber et al. 2004; Fischer et al. 2006; Huggel 2009).

Rock avalanches and other landslides in the Southern Alps have been investigated in a number of studies, but few are regional scale. Studies have examined slope failures associated with earthquakes (e.g. Speight 1933; Adams 1981; Bull and Brandon 1998; Orwin 1998) or affecting road construction (Paterson 1996). Other detailed works describe individual rock avalanches that initiated from high-elevation bedrock slopes about the drainage divide (Main Divide) crest during the past 20 years, including the catastrophic summit collapse of New Zealand's highest mountain, Aoraki/Mount Cook (McSaveney 2002; Hancox et al. 2005; Cox and Allen 2009). The first inventory-based study defining long-term occurrence probability was carried out by Whitehouse (1983) using mostly prehistoric rock avalanches. The average occurrence rate of $>10^6$ m$^3$ rock avalanches is estimated at 1 per 100 years across the entire Southern Alps (Whitehouse and Griffiths 1983), but a rate of 1 per 20 to 30 years is probably more characteristic from shattered rocks and precipitous slopes near the Main Divide of the Alps (McSaveney 2002). More recently, inventories have been developed for landslides in South Westland and Fiordland (Hovius et al. 1997; Hancox et al. 2003; Korup 2005b) and used to examine landslide-related sediment flux. This paper serves to complement existing inventory-based research, within a GIS approach that encompasses the entire central Southern Alps, but more specifically offers the first discussion regarding glacial ice recession, permafrost warming and potential impacts on recent land sliding in this mountainous region of New Zealand.

## Methodology

The quarter-million-scale (QMAP) digital geological map of New Zealand (Rattenbury et al. 1994) is currently being produced by the Institute of Geological and Nuclear Sciences (GNS Science) to supersede a previous 1:250,000 national geological map series published during the 1960s. The QMAP project started in 1994 and now includes the recently completed Aoraki sheet describing the central Southern Alps (Cox and Barrell 2007). QMAP is based on geological information plotted on 1:50,000 topographic base maps, compiled from previous studies and new field work. Data are simplified for digitising at the compilation stage, with line work smoothed and geological units amalgamated to a standard national system, enabling production of 1:250,000 hard-copy maps. Related research applications are best suited for the regional level because of the scales at which data were captured and simplified. Landslides are defined within QMAP as both landslide deposits (within the geological unit layer) and as landslide-affected areas (polygons and arcs in a specific landslide layer). Approximately 25–30% of these landslides has previously been recorded in earlier inventories (Table 1), but was in all instances remapped in the field and/or re-examined from aerial photography to achieve consistency in the QMAP data. Landslides occur on all scales, but, due to the map simplification process, only those larger than 0.02 km$^2$ were digitised, with boundaries smoothed and digitised to an accuracy of ±100 m. In practice, this results in variable uncertainty in landslide area: approximately ±25% for small landslides (<0.1 km$^2$), ±10% for large landslides (1–10 km$^2$) and ±1% for very large landslides (>10 km$^2$). Types of landslide (after Cruden and Varnes 1996) include: shallow translational slides and rotational slumps on lowland hillslopes; deeper-seated earthflows, slides or slumps within Late Cretaceous–Cenozoic sedimentary rocks; large block-slides and landslide complexes in mountain bedrock; and large rock/debris falls from bluffs. In addition, rock avalanches are very rapid to extremely rapid complex falls which develop a fluid-like behaviour (Hungr et al. 2001) and are differentiated in the dataset based on the relative location of deposits and source areas, deposit morphology and composition. Deposits classified as rock avalanches in this study typically have relatively large fall heights (>500 m) and long run-out distances (1,000–4,000 m) and comprise unsorted bouldery, silty, sandy debris (see also Whitehouse 1983). Identification of large, deep-seated landslide complexes is easiest where obvious scarp development and slumping has occurred, which is particularly evident where moraine terraces or other cover sequences have been displaced. However, where this evidence is not obvious, potentially very large landslide complexes which have not developed into a rock avalanche may be missing from the inventory. Smaller, shallow slope failures such as debris flows are clearly evident in forested regions, but become more difficult to recognise in alpine regions, and therefore, older events of this type may also be underrepresented in the inventory.

The QMAP landslide dataset forms the basis for this study, with the addition of several new published (Cox et al. 2008) and unpublished events identified since compilation of Aoraki QMAP. In total, 509 landslides were mapped, 401 of which have no specific failure mechanism defined, and 108 of which were subclassified as rock avalanches. This represents a minimum catalogue of events in the region, particularly for slope failures

**Table 1** Overview of previous landslide inventory studies within central and western regions of the Southern Alps, indicating overlap with the current study

| Author | Location | Research applications | Total study area | Minimum landslide size[a] | Total number of landslides | Landslides included in current study |
|---|---|---|---|---|---|---|
| (Whitehouse 1983) | Central Southern Alps | Magnitude/frequency; geological distribution; sediment delivery | 10,000 $km^2$ | 0.05 $km^2$ | 46 | 31 |
| (Hovius et al. 1997) | Western Southern Alps | Sediment delivery | 4,970 $km^2$ | 0.0001 $km^2$ | 7691 | ~100[b] |
| (Korup 2005b) | Western Southern Alps and Fiordland | Magnitude/frequency; topographic distribution; sediment delivery | 18,670 $km^2$ | 0.01 $km^2$ | 778 | ~100[b] |
| Current study | Central Southern Alps | Geological and topographic distribution; climate change impacts | 21,300 $km^2$ | 0.02 $km^2$ | 509 | – |

[a] Given as total affected area (scarp and deposits combined), except for Whitehouse (1983), which refers to deposit only

[b] The majority of these landslides are common to both Korup 2005b and Hovius et al. 1997

occurring within glaciated terrain or depositing into highly erosive watersheds where geomorphic evidence can rapidly become unrecognisable (Hewitt et al. 2008). For the nonspecific landslides, failure scarps digitised as arcs within the QMAP dataset were enclosed to form polygons approximating the landslide source areas. Rock avalanche source areas were treated to a higher level of discrimination, given that detachment zones were often small and poorly defined by QMAP landslide scarps. Therefore, air-photo and satellite-image interpretation, topographic maps and shaded relief images were used to directly map the source areas for all 108 rock avalanches, verified wherever possible by field observations and with reference to published studies and reports. Source areas were digitised directly on the shaded relief imagery generated from the NZ 25-m grid cell digital elevation model (DEM). Created from 1986 aerial photography and assessed to have a root mean square error of 5–8 m for hilly, steep terrain (Barringer et al. 2002), this DEM provided the basis for all topographic analyses. All complete landslide affected areas and related source areas for the 401 nonspecific landslides, and 108 rock avalanches were linked by a landslide identification code and a combination of zonal statistics and spatial queries used to derive related topographic and geological information for the inventory. Alluvial deposits and flat (<1°) slopes which predominate within valley floors comprise over 40% of the study region and were excluded from all analyses to provide more meaningful results in the context of a slope instability study. The term hillslope is used herein for these non-alluvium areas with slopes ≥1°.

## Physical setting

This study covers 21,300 $km^2$ of the central Southern Alps, centred upon the Aoraki/Mt Cook National Park, but also extending west of the Main Divide of the Southern Alps towards the Alpine Fault, north to the headwaters of Rakaia River and east to include the lower elevation foothills bordering the Canterbury Plains and MacKenzie District (Fig. 1). It encompasses the highest and most heavily glaciated terrain of the Southern Alps while traversing different climatic regimes from superhumid, maritime conditions in the west (precipitation >12 m $y^{-1}$), to a drier, more continental climate towards the east (precipitation <2 m $years^{-1}$) (Griffiths and McSaveney 1983).

The Alpine Fault is a major active fault traversing the northwestern edge of the study area, on which most of the ongoing surface tectonic movement between the Australian Plate (to the northwest) and the Pacific Plate (to the southeast) is concentrated (Fig. 1). Neogene displacement of up to 470 km along the Alpine Fault has brought together two different pre-Cretaceous geological provinces (Cox and Sutherland 2007). Northwest of the Alpine Fault, there are small amounts of exposed Paleozoic metasedimentary and plutonic basement rocks that are fragments of the Gondwanaland supercontinent (Cox and Barrell 2007). Southeast of the Alpine Fault, basement rocks belong to the Torlesse composite terrane. They comprise thick, deformed packages of sandstone and mudstone that were deposited and accreted to Gondwanaland during the Carboniferous to Early Cretaceous and have locally been metamorphosed into greywacke semischist or schist. Convergence across the Australian-Pacific plate boundary pushes thinned and submerged crust upward into the path of a strong westerly atmospheric circulation. Differential uplift, erosion and rock exhumation across the Southern Alps has exposed transitions from uncleaved greywackes in the east, through weakly cleaved or fractured greywacke and foliated semischist about the Main Divide, to strongly-foliated amphibolite facies schist (almost gneiss) in the west adjacent to the Alpine Fault (Fig. 1). Late Cretaceous–Pliocene sedimentary and volcanic tertiary rocks occur locally in the Canterbury foothills, beneath the Canterbury Plains, and locally west of the Alpine Fault. Dextral transpression along the Alpine Fault causes uplift of the Southern Alps by folding and faulting, continuing to the present day at up to 10 mm per year (Norris and Cooper 2001). The entire area is subject to episodic shaking from high-magnitude M7–8 earthquakes every 200–300 years, occurring most recently in ~1717 AD (Wells et al. 1999; Sutherland et al. 2007) and appearing seismically quiescent since observations began in the early 1900s.

Pleistocene–Holocene glacial cycles carved and shaped the central Southern Alps, leaving a mantle of cover deposits throughout the region. Glaciations began at least by the Late

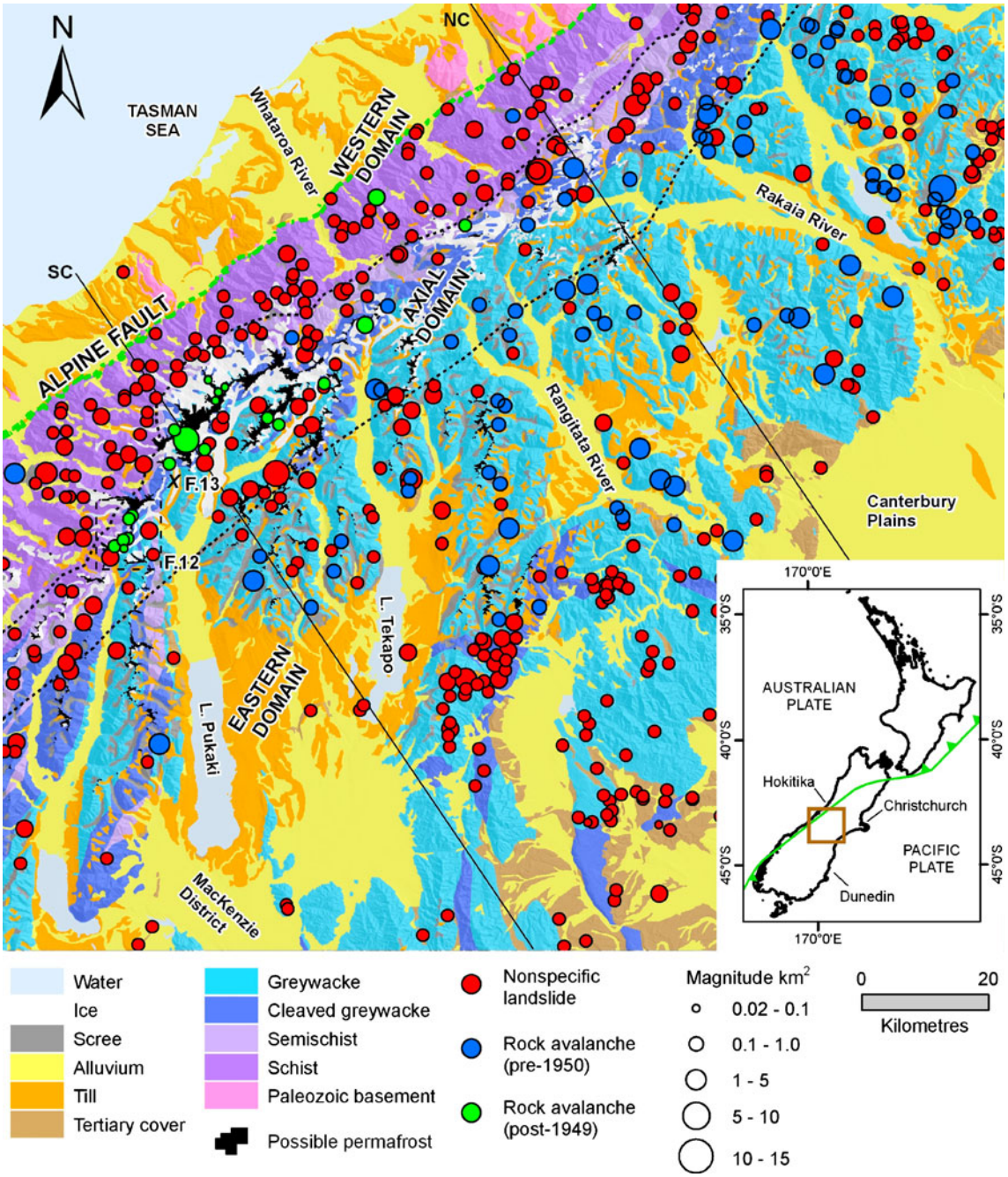


**Fig. 1** Simplified geological classification of the central Southern Alps (after Cox and Barrell 2007), showing landslide distribution in relation to the three main geomorphic domains described by Whitehouse (1988). Permafrost distribution is after Allen et al. (2008b). Northern (*NC*) and southern (*SC*) transects across the Alps relate to Fig. 2c and also indicated are the locations shown in Fig. 12 (Mueller Glacier) and Fig. 13 (Hooker Glacier). Landslide magnitude describes the total affected area (source and deposit areas combined). *Inset* shows the position of the Australian-Pacific plate boundary

Pliocene (Suggate and Wilson 1958) and by the Late Pleistocene, an extensive system of glaciers extended almost uninterrupted 700 km along and 100 km across the Southern Alps (Newham et al. 1999). Glaciers coalesced in the main mountain valleys to form piedmont lobes in the west and extended through the foothills to alluvial outwash plains in the east. Till deposits mark the extent of ice during the last glacial maximum (LGM) around 26–23 ka (calibrated years BP); there is widespread evidence for at least four major periods of glacial re-advance since the LGM (Fitzsimons 1997). Since the end of the little ice age (LIA) in the mid-nineteenth century there has been significant ice-loss (49% decrease in glacier area and 61% decrease in glacier volume; Hoelzle et al. 2007) and the disappearance of many snowfields, despite episodic local advances in response to changes in atmospheric flow patterns (Chinn et al. 2005). Accompanying and contributing to the disintegration of many glacial tongues has

been the formation of large lakes, which continue to grow rapidly in proglacial areas east of the Main Divide (Allen et al. 2009), increasing the potential for flood waves from bedrock failures impacting these lakes (e.g. Bishop and Hislop 1983; McSaveney 2002).

A current estimate of permafrost distribution in the central Southern Alps (Fig. 1) (Allen et al. 2008b) has been calculated on the basis of a topo-climatic key used to describe the lower limits of permafrost occurrence in the European Alps (Haeberli 1975). Physical relationships incorporated in this approach consider aspect-dependent radiation effects and altitudinal changes in air temperature. While precipitation will have a significant influence on ground temperature on flatter slopes, resulting primarily from the insulation properties of long-lasting snow-cover, this factor is considerably reduced or absent on steeper rockwalls (Gruber and Haeberli 2007). However, the precipitation gradient across the Southern Alps and its influence on atmospheric moisture content was accounted for by using local air-temperature records from the past two decades and appropriate free-air lapse rates above three climate stations located across the study region (Allen et al. 2008b). The altitudinal limits given in the original key were calibrated locally from these data and validated on the basis of fossil and active rock-glacier distribution. Although found only in the drier mountain ranges southeast of the Main Divide, rock glaciers can only form and maintain their creeping deformation where perennially negative ground temperatures are sustained over sufficiently long time scales and therefore provide a reliable proxy for paleo- or more recent permafrost. On steep, largely snow-free shaded aspects near the Main Divide, the lower limit of permafrost occurrence is estimated at 2,300 m, rising to over 3,000 m on sunnier aspects, while a drier climate and higher free-air lapse rates are estimated to lower these limits by ~300 m further towards the southeast (Allen et al. 2008b). Long climate records from Hokitika (West-Coast) are often used as a proxy for the general climate of the central Southern Alps; warming of 0.7°C was documented for the period 1920–1990 (Salinger et al. 1995), suggesting slowly degrading permafrost may exist 100–150 m below the current estimated permafrost limits. Climate data from Aoraki/Mount Cook village located east of the Main Divide also support a general warming trend that has continued into the twenty-first century (Huggel et al. 2010).

## Regional topography

Elevations of central South Island extend from sea level up to the highest peaks of the Mount Cook massif above 3,700 m. Local relief near the Main Divide rises 1,000–2,700 m within a horizontal distance of less than 5 km. A large proportion of the land area is within lowland valleys where fluvial processes dominate, and slope angles are low. Above 1,000 m, hillslope area decreases with elevation, such that only 6% of all slopes are located at elevations above 2,000 m (Fig. 2a). However, the higher-elevation slopes are progressively steeper and more extensively covered by perennial ice (Fig. 2b), with modal ($\phi$) and mean ($\psi$) slope gradients in excess of 45° characterising the highest slopes in the vicinity of the Main Divide. Between 1,000 and 2,000 m in the Southern Alps, $\phi$ is relatively constant at 33–34°, with only a small increase in $\psi$ from 29–31°. Although located at a higher elevation, this zone has slope characteristics similar to the subalpine domain identified west of the Main Divide, where

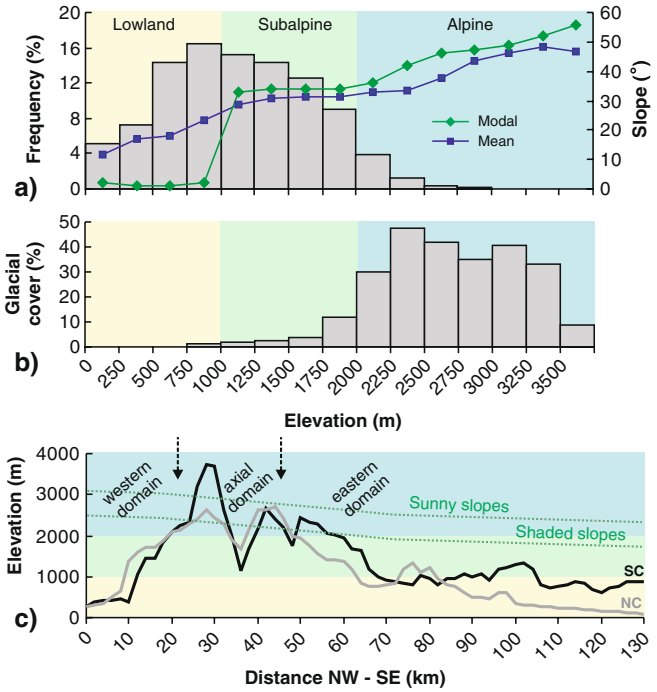


**Fig. 2** **a** Hillslope frequency distribution and slope angles calculated in 250-m elevation increments, with three altitudinal zones identified (*coloured*). **b** Proportion of perennial ice cover out of total hillslope area with respect to elevation. **c** Southern (*SC*) and Northern (*NC*) maximum elevation transects across the central Southern Alps (refer to Fig. 1), showing general altitudinal zones (*coloured*) and lower limits of permafrost distribution (*green dashed*, after Allen et al. 2008b). The approximate separation of the three main geomorphic domains described by Whitehouse (1988) are indicated by *arrows*

Korup et al. (2005) considered mass movement and fluvial erosion/sedimentation to be the dominant geomorphic processes. The effects of relief damping by glacial ice cover that were described for the Alpine zone (Korup et al. 2005) are not distinguishable within the larger study area. In addition, there are no clear transitional changes in slope above 2,000 m, and therefore, a single alpine altitudinal zone is used here to refer to steep terrain above 2,000 m. Ablation areas of the larger valley glaciers extend below 1,000 m east of the divide and nearer to sea level for glaciers in the west, such as Franz Josef and Fox Glaciers. Whitehouse (1988) described three main geomorphic domains occurring across the central Southern Alps, resulting from differential tectonic uplift, precipitation, erosion and glaciation. These domains provide a basis for analyses considering topographic and landslide-related variances across the Alps, but also correspond well with estimated permafrost distribution across the region (Figs. 1 and 2c). In the western domain, permafrost is unlikely to occur, becoming more frequent about Alpine slopes in the axial domain and restricted to the highest-shaded slopes in the eastern domain where the only active rock glaciers are found (Brazier et al. 1998).

For the purpose of analysing landslide distribution in relation to geological setting, a simplified geological classification scheme was developed (Table 2), reflecting both the metamorphic bedrock gradation that occurs southeast of the Alpine Fault, and the existence of various cover sequences

**Table 2** Simplified geological classification scheme derived for the central Southern Alps

| Class | Description | Regional coverage, % |
|---|---|---|
| Water | Surface water on land–lakes and lagoons | 2 |
| Cover | | |
| Ice | Glaciers (digitised from 1986 aerial imagery) | 3 |
| Scree | Talus and colluvium on hillslopes, including some hanging-valley till deposits either >50 m thick or, >1 $km^2$ areal extent | 3 |
| Alluvium | Fan gravels and outwash alluvium, infilling major valley floors | 34 |
| Till | Thick glacial sequences and moraine deposits >50-m thick | 12 |
| Tertiary cover | Late Cretaceous–Pliocene sedimentary and volcanic rocks | 3 |
| Bedrock | | |
| Greywacke | Interbedded sandstone, siltstone and argillite of the Torlesse composite terrane | 27 |
| Cleaved greywacke | Weakly developed cleavage evident | 6 |
| Semischist | Cleaved and weakly schistose greywacke and argillite of the Torlesse composite terrane | 2 |
| Schist | Strongly foliated schist (almost gneissic), containing greenschist or amphibolite facies metamorphic mineral assemblages | 7 |
| Paleozoic basement | Meta-sedimentary and plutonic basement rocks northwest of the Alpine Fault | 1 |

resulting from glacial, periglacial and fluvial processes. Over half of the region is mapped by QMAP as cover formations (exceeding 50 m in depth, or 1 $km^2$ areal extent), which are predominantly alluvium and till deposits. The remaining landmass consists of bedrock slopes either exposed or inferred where the depth or areal extent of surface cover are considered less, with greywacke predominating in vast areas east of the Main Divide. The distribution of bedrock units is non-uniform with slope aspect (Fig. 3a). Schist and semischist bedrock is exposed more frequently on slopes facing north through to southwest, while greywacke is mapped relatively evenly across all slope aspects. The higher proportion of cleaved greywacke on east- and southeast-facing slopes reflects uplift and exposure of these rocks in the hangingwall of west-dipping faults, such as the Main Divide Fault Zone (Cox and Findlay 1995) and Great Groove Fault in the Sealy Range (Lillie and Gunn 1964). Schist and semischist rocks are almost entirely exposed west of the Main Divide and exhibit slopes that are noticeably steeper than greywacke and cleaved greywacke for many aspects (Fig. 3b). The steepest schist and semischist slopes occur on northeast and east aspects.

## Landslide distribution

### Overview

Nearly 2% (414 $km^2$) of the total land area in the central Southern Alps is affected by landsliding. Although the precise age of most landslides is poorly known, the majority of shallow and small-scale failures preserved in this rapidly evolving landscape are assumed to be relatively young features, mostly activated during the Holocene (<12 ka). At the least, slope failures recognised within the ice limits from the last glacial maximum (Cox and Barrell 2007) are thought to have occurred since the withdrawal of this ice (~26 ka), as earlier deposits would have been notably modified or removed by glacial cycles. Commonly, unmodified hummocky deposits are evident, and in other instances, immature soil development provides further evidence for Holocene-aged deposits. However, it is recognised that Pleistocene glacial cycles also carved and shaped the landscape, and some deep-seated landslides may have been initiated during this time. For the purpose of exploring recent climate influences, distinction is given here to failures initiated during the past 100 years, primarily as rock avalanches. Within the subsequent analyses, three datasets

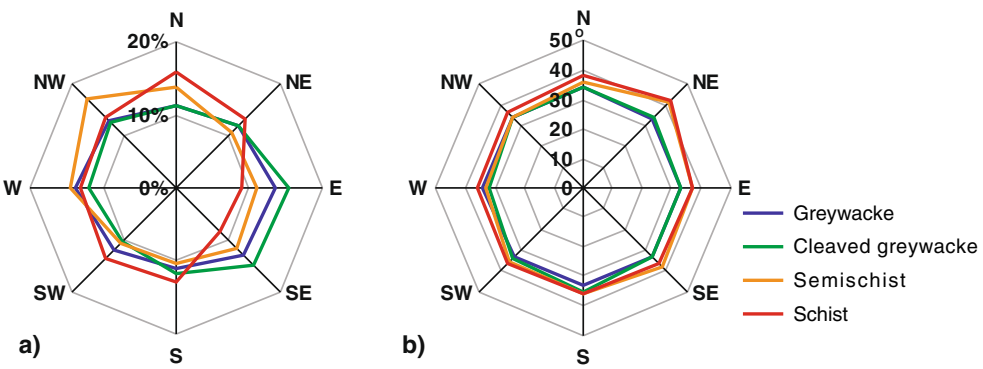


**Fig. 3** **a** Distribution of exposed bedrock and **b** modal bedrock slope angle as a function of aspect. Based on QMAP geological units (Cox and Barrell 2007)

are therefore referred to; 'rock avalanche post-1949' analyses are based on the 20 source areas identified from the most recently mapped failures; 'rock avalanche pre-1950' analyses include 88 older and undated failures; 'nonspecific landslide' analyses are based upon the source areas of the remaining 401 landslides for which no other specific failure type has been assigned.

The distribution of landslides is centred upon the mountainous terrain and foothills both east and west of the Main Divide, with flat lowland areas such as the Canterbury and Mackenzie District plains largely unaffected by landslide activity (Fig. 1). The average spatial density of nonspecific landsliding is highest for hillslopes in the western domain, with one event per 25 $km^2$, decreasing to one per 27 $km^2$ in the axial domain and one per 37 $km^2$ in the eastern domain. The combined average spatial density of all rock avalanches is less, with the highest density recognised in the axial domain of one event per 72 $km^2$, compared with 1 per 123 $km^2$ further east.

The size of mapped landslides (source and deposit areas combined) ranges from 0.02 $km^2$ to more than 14 $km^2$, with a common size distribution shared between pre-1950 rock avalanches and other nonspecific landslides (Fig. 4). Post-1949 rock avalanches show a higher proportion of smaller events in the range of 0.02 to 0.25 $km^2$. Over 20% of all slope failures included in the inventory (rock avalanche or nonspecific landslide) can be arbitrarily labelled large (>1 $km^2$), and these events constitute 57% of the total landslide-affected area. No landslide volumes are included in the inventory because pre-failure topography cannot be reconstructed in most cases. However, slope failures from recent decades provide an indication of the large magnitudes that have been involved in rock avalanches such as Aoraki/Mt Cook ($12\times10^6$ $m^3$; McSaveney 2002) or Mt. Adams ($10–15\times10^6$ $m^3$; Hancox et al. 2005) or even larger volumes involved in complex landslides such as the ongoing failure beneath the Mueller Hut on the Sealy Range (>$100\times10^6$ $m^3$; Cox and Barrell 2007).

## Geology

The lithology characterising rock avalanche (pre-1950 and post-1949) and nonspecific landslide source areas shows clear differentiation (Fig. 5). The predominant lithology is calculated as the geological unit that contributes the majority of source area cells (25-m pixels) for each recorded rock avalanche or nonspecific landslide, normalised by total area for each geological unit. Nonspecific landslides have occurred from the largest range of

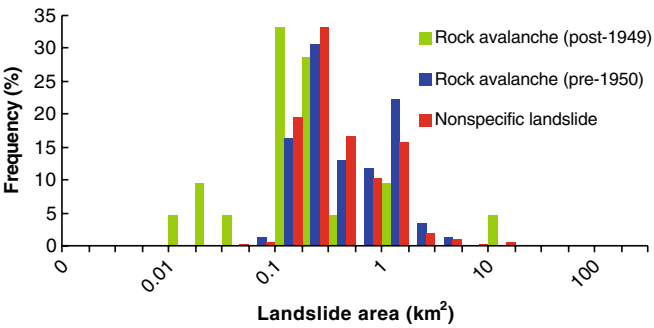


**Fig. 4** Frequency distribution of landslide area (scarp and deposit areas combined) as mapped for the central Southern Alps

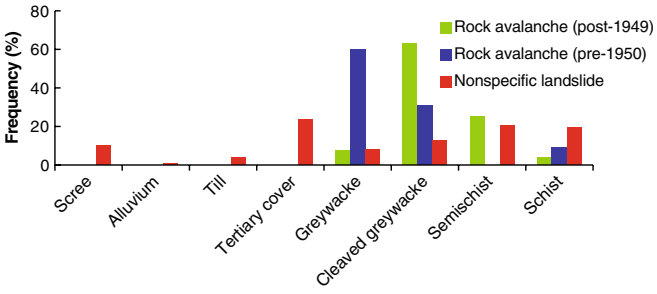


**Fig. 5** Area normalised landslide distribution as a function of source area bedrock or cover lithology

lithologies, corresponding with their wide distribution from west to east across the entire central Southern Alps (Fig. 1). Scree has formed within or beneath some of these landslide scars, and till has been displaced within large landslide complexes where downwasting of valley glaciers has destabilised adjacent lateral moraines (Blair 1994). In some notable instances above the Tasman, Murchison and Mueller Glaciers, active landslide scarps occur large distances uphill where bedrock has also been destabilised in response to glacial recession. The area-normalised occurrence of nonspecific landsliding is highest from tertiary rocks which form lowland hillslopes bordering the Canterbury Plains and high metamorphic-grade semischist and schist slopes, mostly occurring west of the Main Divide (Fig. 5). In the west, shallow debris failures and very large, slow failure of entire hillslopes are thought to be common landslide mechanisms, accounting for an average 9±4 mm $year^{-1}$ denudation (Hovius et al. 1997) and contributing exceptional sediment delivery to rivers draining the wetter, windward side of the Southern Alps (Korup et al. 2004; Korup 2005b). This geological association is reversed for pre-1950 rock avalanche activity, with source areas most evident from greywacke slopes which predominate east of the Main Divide (Fig. 5). Rock avalanches post-1949 have occurred most frequently from cleaved greywacke and semischist slopes which predominate about the higher elevation axial domain of the Southern Alps, where the hangingwall of the Main Divide Fault Zone overlies greywacke of the footwall. Although geomorphic evidence has been less commonly observed, large rock avalanches can occur from schist slopes in the west, as illustrated by the catastrophic 1999 failure of Mt. Adams (Hancox et al. 2005), which remains the only recent rock avalanche recorded outside of the axial domain, within the study region.

## Topographic distribution

The distribution of both pre-1950 rock avalanche and nonspecific landslide source areas predominates from slopes orientated west to northwest across all geomorphic domains of the central Southern Alps (Fig. 6a–c). This trend is most pronounced for slopes within the axial domain of the Alps, where 66% of all nonspecific landslide source area cells are observed on west to northwest facing slopes, and over 30% of all pre-1950 rock avalanche source areas are orientated towards the northwest (Fig. 6b). In contrast, rock avalanches observed post-1949 within the axial domain show a distinct prevalence from source areas facing east to southeast (75%), highlighting the significant number

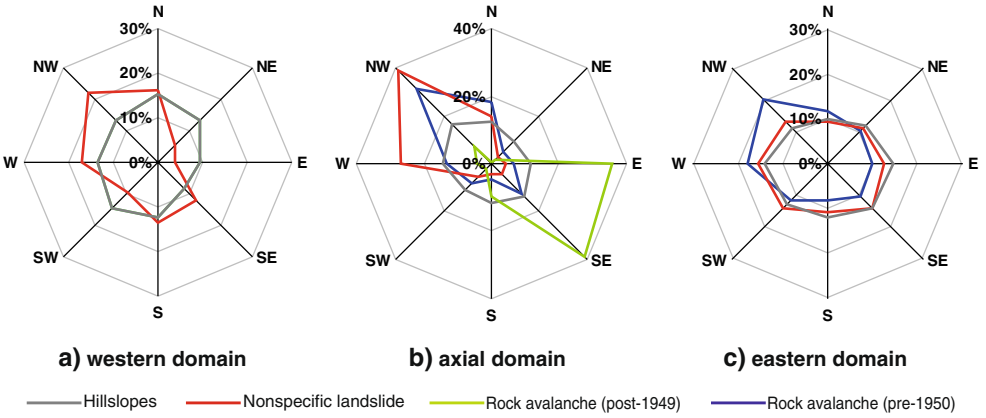


**Fig. 6** **a**–**c** Distribution of all hillslopes and landslide source areas as a function of slope aspect across three geomorphic domains of the central Southern Alps. Rock avalanche distributions are not shown in all graphs, as in some domains there are insufficient numbers to be meaningful (e.g. neither pre-1950 or post-1949 events are indicated for the western domain, as only three rock avalanches are mapped in this region—see Fig. 1)

of recent failures that have occurred from rocks dipping towards the west in the exposed hangingwall of the Main Divide Fault Zone.

Within the western and axial domains, source-area slope angles for nonspecific landslides ($\phi$=32°), appear lower than general hillslope angles ($\phi$=36°; Fig. 7a). In part, this may reflect the predominance of nonspecific landslides occurring from within lowland to subalpine elevation zones (Fig. 8.), where hillslope angles are lower than at higher elevations, but may also result from the displacement and reduction in slope caused by large landslides (Korup 2005b). In the eastern domain, a closer correspondence between modal hillslope angles and slope measured within nonspecific landslide source areas is observed ($\phi$=32°). Lower hillslope angles in the eastern domain probably reflect the greater presence of slopes comprising weaker till or tertiary rocks (see Fig. 1). Pre-1950 rock avalanche source areas in the eastern and axial domains are typically steeper ($\phi$=35°), sometimes creating convex cirque-like depressions where deep-seated failures have occurred (Turnbull and Davies 2006; Fig. 7b). In the axial domain, post-1949 rock avalanches have detached from extremely steep surfaces, with over 65% of source areas cells being steeper than 45°, reflecting a large number of failures occurring from generally steeper, higher elevation slopes (Fig. 8), where many precarious scarps have been exposed near or at ridgelines. Slope angle is frequently incorporated in landslide susceptibility analyses (e.g. Donati and Turrini 2002; Pike et al. 2003). Results here indicate a notable increase in the proportion of pre-1950 and particularly post-1949 rock avalanche failures occurring from slopes >50°, relative to general hillslope distribution (Fig. 7b). This relationship is not evident for nonspecific landslide source areas because the various failure types involved in these cases operate across a wider range of lithologies (Fig. 5) and originate from within a lower elevation range (Fig. 8) where modal slope angles are generally lower. For higher elevation,

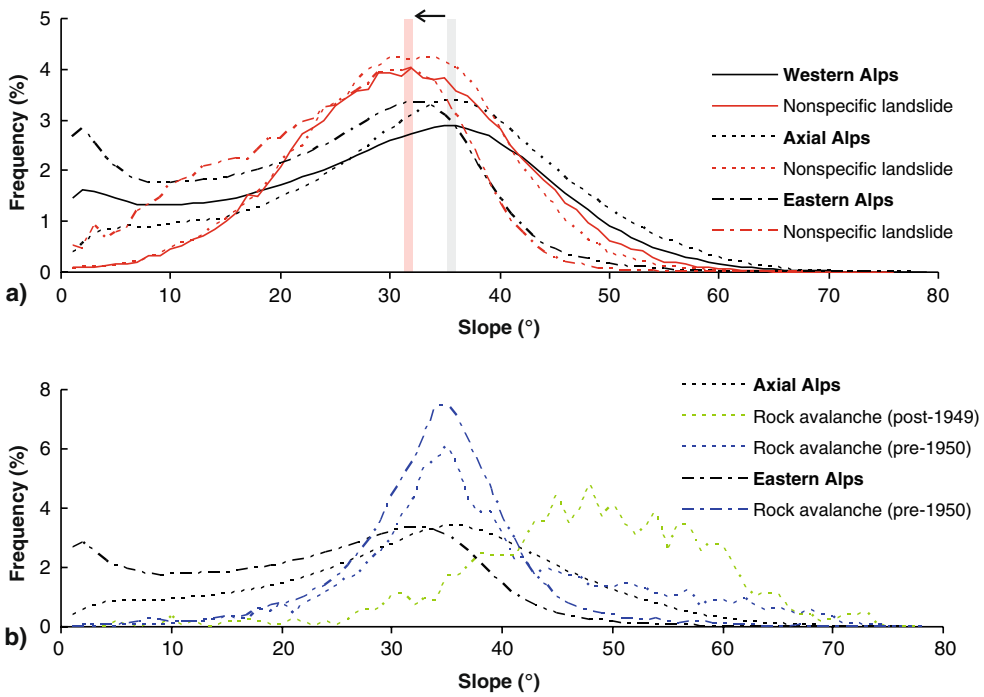


**Fig. 7** **a** Slope–frequency distributions for all hillslopes and nonspecific landslide source areas across three geomorphic domains of the central Southern Alps, with *coloured bars* indicating the decrease in modal slope for landslide source areas relative to general hillslope angles. **b** Slope frequency distributions for all hillslopes and rock avalanche source areas in the axial and eastern domains only

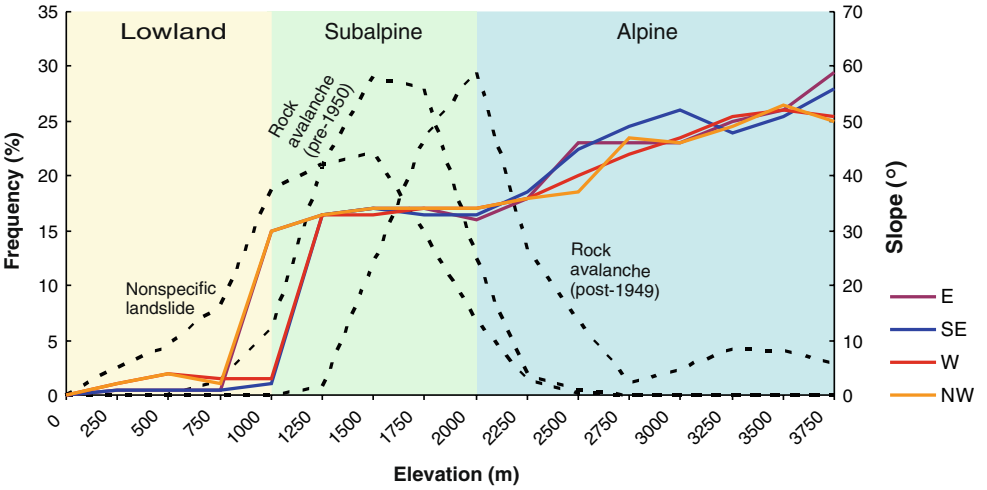


**Fig. 8** Modal slope as a function of aspect calculated within 250 m elevation increments, compared with the frequency distribution of landslide source area cells. The exposure of hangingwall rocks between ~2,000 and 3,000 m creates notably steeper slopes on east–southeast aspects. *Coloured* altitudinal zones correspond with Fig. 2

typically steeper, alpine slopes, rock avalanching and higher frequency/lower magnitude rockfalls appear to be the dominant modes of slope failure.

### Glacial change and slope stability

#### Recent rock avalanche distribution

Extending back to the mid-twentieth century, a comprehensive record of rock avalanches has been observed in the central Southern Alps, with these failures predominating from steep Alpine slopes about the axial domain of the Main Divide (see Fig. 1). No slope failures dating from earlier in the twentieth century have been mapped, and therefore the record of landsliding from the past 100 years is limited to post-1949 data. In considering the possible influences of twentieth century permafrost recession and glacial retreat, emphasis is given here to the distribution of these recent rock avalanches, relative to mapped or modelled zones of perennial ice and permafrost in the central Southern Alps (Fig. 9). The glacial zone in this context is indicated by the steady-state glacier equilibrium line altitude, defining the longer-term elevation above which ice accumulation is favoured over ablation, and above which the proportion of perennially ice covered slopes increases significantly (Fig. 2b). Because of strong precipitation gradients, this elevation rises steeply from ~1,600 m west of the Main Divide to over 2,200 m in the east and includes possible variations of up to 200 m from sunny northern to shaded southern slope aspects (Chinn 1995). While it appears that rock avalanches have only occurred from higher elevation slopes during the past century (Fig. 9), this is considered to be an observational bias, with earlier events depositing onto glaciers not being recognised and therefore missing from the inventory. Debris from prehistoric rock avalanches may now be incorporated into terminal moraines, where distinguishing deposits derived from earthquakes and/or past climatic regimes may be difficult (e.g. Larsen et al. 2005; Shulmeister et al. 2009). In addition, many prehistoric rock avalanches are located east of the Main Divide where fewer high-elevation slopes exist, and the spatial distribution of these failures is likely to be biased by earthquake-generated members (see

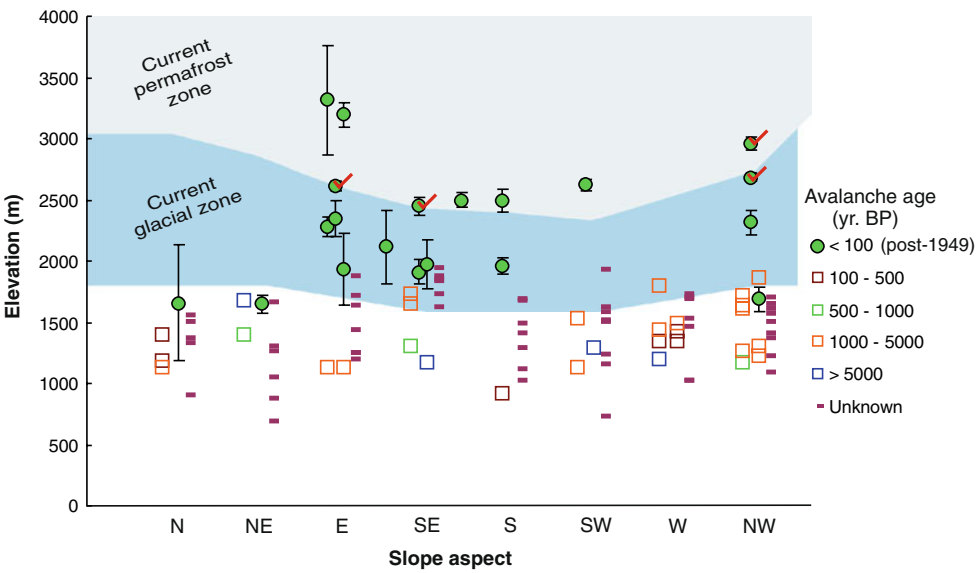


**Fig. 9** Mean elevation of 108 rock avalanche source areas in the central Southern Alps. The maximum and minimum elevations of the source area for the post-1949 events are also indicated (*bars*), with *red ticks* denoting events that occurred during the warm dry summer of 2007/2008 (Table 3). The estimated permafrost zone is indicated for the Main Divide (after Allen et al. 2008b) and overlaps with the glacial zone. Dates older than 100 years. BP are predominantly after Whitehouse (1983)

**Table 3** Significant rock avalanches and rockfalls recorded in the central Southern Alps over the past 100 years

| Location | Date | Max elevation source (m) | Min elevation source (m) | Slope aspect source | Median slope source (°) | Source lithology and collapse structure | Estimated permafrost lower limit (m) | Glacial conditions[a] | Total area ($km^2$) | α (°)[b] | Reference |
|---|---|---|---|---|---|---|---|---|---|---|---|
| Mt. Isobel I | 1950–1955 | 2,180 | 1,780 | SE | 47 | Cleaved greywacke, scarp slope | 2,440 | Gl. directly above<br>Gl. ~280 m below | 0.66 | 23 | McSaveney 2002 |
| Mt Isobel II | c. 1965 | 2,360 | 2,200 | E | 59 | Cleaved greywacke, scarp slope | 2,590 | Steep glacial ice<br>Gl. directly below | 0.25 | 30 | McSaveney 2002 |
| Mt Vancouver | 1974–1975 | 3,300 | 3,100 (uncertain) | E | 61 | Greywacke, scarp slope | 2,590 | Steep glacial ice | - | - | McSaveney 2002 |
| Murchison Glacier[c] | 25/12/75 | 1,820 | 1,590 | NW | 33 | Greywacke, partly dip slope | 2,690 | Gl. directly below | 0.43 | 11 | Whitehouse and Griffiths 1983 |
| Beelzebub Glacier | 1980–1984 | 2,030 | 1,900 | S | 42 | Cleaved greywacke, dip slope | 2,390 | Gl. directly below | 0.24 | 18 | Korup 2005a |
| Aoraki/Mt Cook | 14/12/91 | 3,760 | 2,870 | E | 51 | Greywacke, scarp slope | 2,590 | Steep glacial ice and hanging glaciers | 14.6 | 22 | McSaveney 2002 |
| Mt Fletcher I & II[d] | 02/05/92<br>16/09/92 | 2,420 | 1,810 | E/SE | 50 | Cleaved greywacke, scarp slope | 2,590–2,440 | Steep glacial ice<br>Gl. ~100 m below | 2.22 | 22 | McSaveney 2002 |
| La Perouse | 1994–1995 | 2410 | 2220 | NW | 47 | Greywacke, dip slope | 2690 | Steep glacial ice<br>Gl. ~200 m below | 0.37 | 29 | This study |
| Mt Thomson I | 22/02/96 | 2,230 | 1,640 | E | 59 | Cleaved greywacke, scarp slope | 2,590 | Gl. directly above<br>Gl. directly below | 0.30 | 42 | McSaveney 2002 |
| Mt Thomson II | 2002–2004 | 2,470 | 2,200 | E | 51 | Cleaved greywacke, scarp slope | 2,590 | Steep glacial ice<br>Gl. directly below | 0.17 | 37 | This study |
| Mt, Adams | 06/10/99 | 2,130 | 1,190 | N | 47 | Schist, scarp slope | >3,000 | Gl. on opposing slope facet | 14.7 | 37 | Hancox et al. 2005 |
| Vampire Peak I | 2003 | 2,560 | 2,440 | SE/S | 65 | Semischist, joint controlled scarp slope | 2,440–2,390 | Gl. ~200 m below | 0.42 | 24 | Cox et al. 2008 |
| Mt Beatrice | 23/11/04 | 1,720 | 1,580 | NE | 53 | Cleaved greywacke, toppled scarp slope | 2,840 | Gl. ~100 m below | 0.18 | 20 | Cox et al. 2008 |
| Anzak Peaks (rockfall) | 2007–2008 | 2,008 | 1,810 | SE | 43 | Cleaved greywacke, scarp slope | 2440 | Gl. ~50 m above<br>Gl. ~700 m below | - | 41 | This study |
| Vampire II | 7-13/01/08 | 2,520 | 2,380 | SE | 73 | Semischist, joint controlled scarp slope | 2440 | Gl. ~100 m below | 0.49 | 28 | Cox et al. 2008 |
| Douglas Peak | 18/02/08 | 3,010 | 2,910 | NW | 56 | Greywacke, dip slope | 2,690 | Gl. ~230 m below | 0.03 | 46 | Cox et al. 2008 |
| Mt Spencer | 6-7/04/08 | 2,720 | 2,650 | NW | 53 | Greywacke, dip slope | 2,690 | Gl. ~100 m below | 0.05 | 34 | Cox et al. 2008 |

| | | | | | | | | | | | |
|---|---|---|---|---|---|---|---|---|---|---|---|
| Mt Halcombe I & II[d] | 24/04/08 /01/09 | 2,650 | 2,570 | E | 45 | Cleaved greywacke, scarp slope | 2,590 | Gl. directly below | 0.02 | 35 | Cox et al. 2008 |
| Malte Brun | 01/01/09 16/02/09 | 2,590 | 2,400 | S | 58 | Greywacke, Scarp slope | 2,390 | Gl. directly above<br>Gl. directly below | 0.38 | 21 | This study |
| Mt Barnicoat | 01/11/09 08/03/10 | 2,670 | 2,580 | SW | 56 | Greywacke, scarp slope | 2,340 | Gl. ~100 m below | 0.02 | 38 | This study |

[a] Presence of ice in the source area and ice proximity measured above and below the mapped source area, based on 2006 perennial ice mapping (after Allen et al. 2008a)

[b] $\alpha$ or Fahrböschung—angle of reach measured from avalanche source to toe of the deposit

[c] Rainfall triggered event

[d] Events originated from a common source area

Section 8). However, these considerations do not detract from the clear predominance of recent rock avalanches originating from glaciated slopes and/or permafrost terrain (Fig. 9).

Of the 20 events recorded post-1949, over half have initiated from source areas where the base elevation of the failure has been above 2,000 m and only two have involved sources areas located entirely below 2,000 m (Table 3). One of these lower elevation exceptions was a rainfall triggered failure from a slope above the downwasting Murchison Glacier and the other from beneath Mt. Beatrice where the retreat of the Hooker Glacier since the LIA has exposed the flank of a steep, U-shaped valley wall. These 20 recent events have initiated from a wide variety of collapse structures, span a wide range of magnitudes, feature steep failure slopes (42–73°) and have all had source areas located either directly above or below, or within a close proximity to large valley or smaller mountain glaciers (Table 3). Only in relation to the catastrophic failure of schist rocks from Mount Adams (Hancox et al. 2005) can any recent influence of glacial recession or permafrost degradation be considered extremely unlikely.

Geospatial, pixel-based analyses reveal the highest proportion of slopes affected by post-1949 rock avalanche failure are located between 100–200 vertical or horizontal metres from glaciers (based on 1986 aerial imagery), corresponding with a zone in which modal bedrock slope angles are also steepest (Fig. 10). The proportion of bedrock affected by failure then rapidly decreases at distances beyond 300 m from glacial ice. To test the significance of this relationship, the proportion of bedrock slopes affected by post-1949 rock avalanche failure within 200 m of glacial ice was compared with the proportion of failure observed from all other bedrock slopes about the axial domain of the Alps (Fig. 11a). Comparisons were completed for different slope ranges, confirming a significantly higher proportion of recent failure occurring from glacier-adjacent slopes in all instances. Because a majority of these rock avalanches have been recorded since 1986; further glacial retreat during the past two decades must be considered, although occurring at a much reduced rate than was observed prior to 1986 (e.g. Chinn et al. 2005; Hoelzle et al. 2007).

The mean elevation difference between post-1949 rock avalanche source areas and the estimated lower permafrost boundary is 240 m, with a total of 13 events occurring from within 300 m of this lower boundary, where degrading permafrost is expected (Fig. 9). If only the base level of the source area is considered, eight events are identified within 300 m of the lower permafrost boundary, including all four rock avalanches that occurred during summer 2007/2008 (Cox and Allen 2009). Although this lower permafrost boundary remains only an estimate, the proportion of recent rock avalanche failure observed within ±300 m of this lower limit is significantly greater than the proportion observed from all other bedrock about the axial domain of the central Southern Alps, for slopes less than 60° (Fig. 11b). For steeper slopes, based on a limited number of observations at present, no statistically significant difference can be determined. The 1991 summit failure of Aoraki/Mt. Cook and an earlier event from Mt. Vancouver at 3,300 m initiated from very high elevations where such steep slopes are most frequent. In these instances, warming permafrost was unlikely to be a factor, although high-

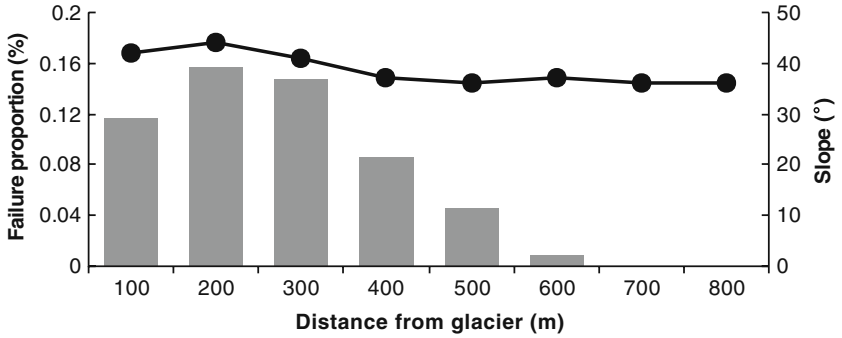


**Fig. 10** The proportion of bedrock within the axial domain of the central Southern Alps affected by post-1949 rock avalanche failure (*grey*, based on mapped source areas) and modal hillslope angle (*black*), relative to glacier proximity

elevation rainfall or the presence of hanging glaciers and percolating firn melt-water may produce subsurface warm thermal anomalies even in very cold environments (Haeberli et al. 2004; Huggel 2009).

### Mueller Glacier and recent slope instabilities

The Mueller glacial valley contains several recent rock avalanche deposits (see Fig. 1) and may exemplify geological and glacial conditions occurring about the Main Divide. The steep, pervasively fractured hangingwall rocks of the Main Divide Fault Zone are cross-cut by numerous secondary faults, partially covered by steep poly-thermal cliff and hanging glaciers and >1,000 m of lateral support has been removed from the valley flanks since the LGM (McSaveney 2002). Historical glacial extents were reconstructed using aerial photography from the years 1965 and 1986, and compared to satellite-based glacial mapping from 2006 (Allen et al. 2008a). Together with estimated permafrost distribution, this information can be compared with the source areas identified from a sequence of spontaneous rock avalanches occurring since the mid-twentieth century (Fig. 12). Both Mt. Thompson events

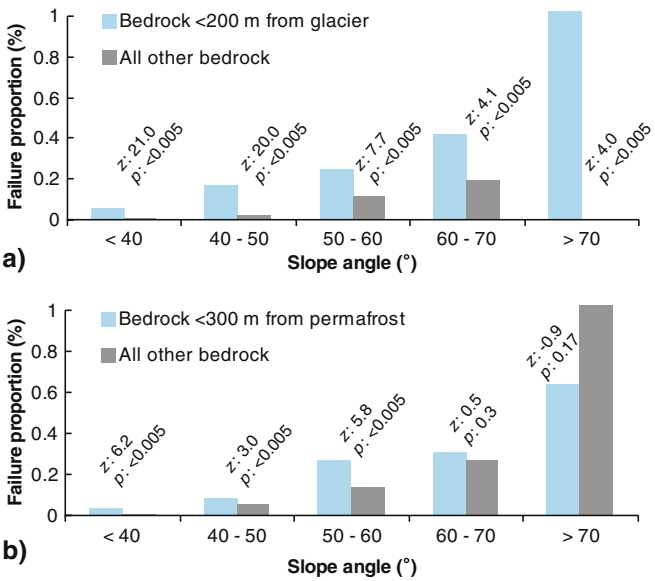


**Fig. 11** The proportion of bedrock affected by post-1949 rock avalanche failure (based on mapped source areas), as a function of slope angle. Significance tests comparing the two proportions in each slope range were calculated from z-scores, with *p*-values <0.01 indicating significant difference at the 99% confidence level. In most cases, *p*-values <0.005 were established

appear to have originated from within zones where some loss of perennial ice cover is evident between 1965 and 1986, while the earliest Mt. Isobel event originated from steep slopes approximately 400 m above the downwasting Mueller Glacier. In contrast, there is no notable loss of perennial ice visible near the source areas of the 1965 Mt. Isobel or more recent Vampire Peak events. However, these failures are positioned within and adjacent to estimated zones of marginal permafrost. The 2008 Vampire Peak event may be significant given that it occurred following a prolonged period of >0°C air temperature at the elevation of the failure and was the first of a sequence of high-elevation rock avalanches to occur during a particularly warm and dry summer (Cox et al. 2008). Qualitative accounts referred to the abnormally rapid melt of snow/ice during the summer and several local guides and helicopter pilots reported unusually high rockfall frequencies, including from beneath the Anzak Peaks area (Table 3). Smaller rockfalls and debris avalanches from the steep formerly glacier-supported walls above the Mueller Glacier are widespread (e.g. Mt. Bannie, Fig. 12), and help maintain a thick supra-glacial debris cover. By comparison, a large and complex deep-seated landslide on the true right of the glacier is inferred to have been creeping slowly since at least the LGM (Cox and Barrell 2007) and possibly during earlier glacial cycles when ice retreat has removed support from the toe of this slope.

## Discussion

Slope-failure mapping across the central Southern Alps shows that most, but not all, rock avalanches have occurred from steep greywacke slopes about and east of the Main Divide. Other landslide types were observed more commonly within the schist and semischist of the western domain, where long-term uplift and erosion are highest (Whitehouse 1988; Fitzsimons and Veit 2001), slope instability is influenced by weakening along the Alpine Fault (Korup 2004) and precipitation is near its maximum (Griffiths and McSaveney 1983). This pattern, however, is influenced by erosion censoring. In the east, large glaciers can remove landslide deposits, while in the west, both glacial and highly erosive fluvial systems combine to influence the longevity of landslide deposits. Many steep, joint-bounded slopes both east and west of the Main Divide must have given rise to catastrophic slope failures, for which no depositional evidence remains. Where evidence has been mapped, other important limitations associated with this regional-scale GIS-based study relate to the generalisation of geological units and simplified assessment of detachment surfaces using zonal statistics. Defining and analysing landslide source areas as 'zones' enabled a larger area of cells to

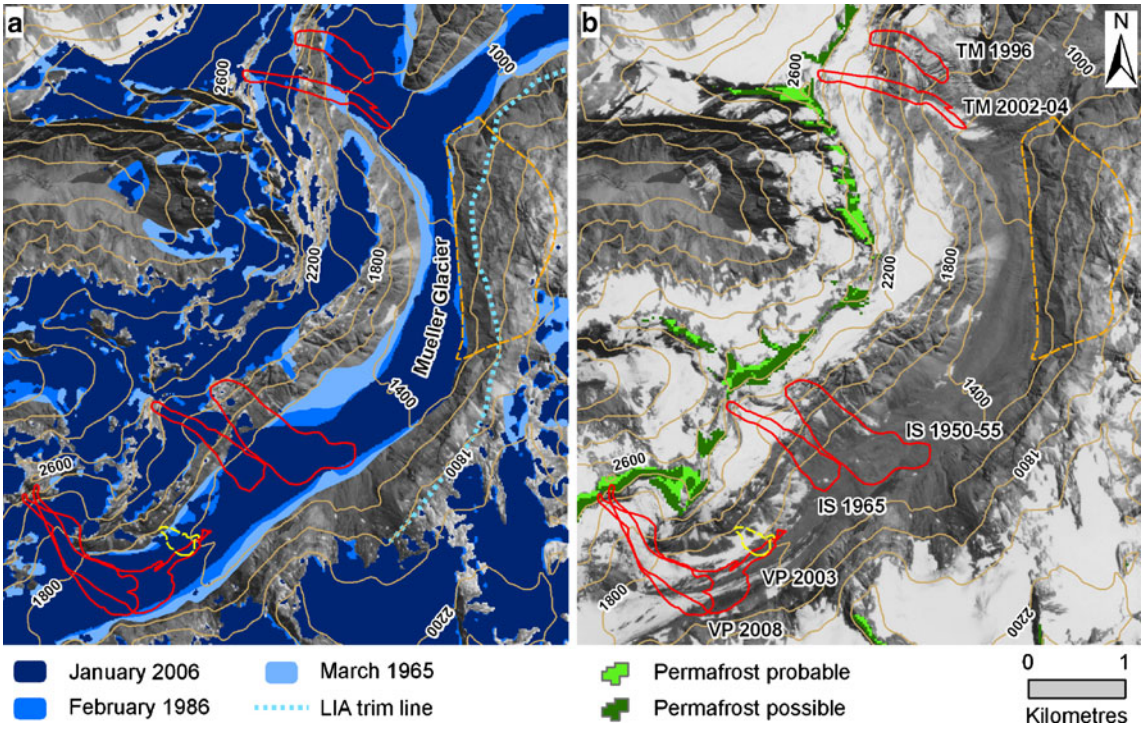


**Fig. 12** Recent rock avalanches occurring from Mt. Thomson (TM), Mt Isobel (IS), and Vampire Peak (VP), Mueller Glacier, Aoraki/Mt Cook National Park, with year of failure indicated. **a** Rock avalanches shown in relation to changing perennial ice extent from 1965 to 2006. **b** Rock avalanches shown in relation to zones of probable and possible permafrost (after Allen et al. 2008b). The zone of possible permafrost is expected to be characterised by thawing permafrost, approaching 0°C. Also indicated is a recent rockfall onto the Mueller Glacier from beneath Mt. Bannie (*yellow dashed*), and a large active, deep seated landslide propagating from the crest of the Sealy Range (*orange dashed*)

be sampled for each slope failure than would have been possible using only digitised scarps, and the influences of spurious values (resulting from positional errors) were minimised using modal and median zone values. Although important slope angle, slope aspect and lithological variations within a source area might be better distinguished using a more sophisticated approach, the use of zonal statistics better suits the resolution of the underlying topographic and geological data. For example, slope angle is calculated over three 25-m pixels, and therefore even the most accurately digitised head-scarp is unlikely to be represented at this scale.

The predominance of all landslide source areas from slopes orientated west–northwest suggests a structural control on landslide distribution in the central Southern Alps (Fig. 6). From the small catalogue of recent events occurring post-1949 (Table 3), there is no clear tendency towards dip-slope failures but important unanswered questions relate to the role of co-seismic landsliding. Considering the importance of co-seismic landsliding established elsewhere in New Zealand (e.g. Pearce and O'Loughlin 1985; Crozier et al. 1995; Hancox et al. 2003), seismicity must also be considered a primary predisposing factor and trigger of slope failure throughout the central Southern Alps. As the recent record presented here contains no earthquake-generated landslides, it may be postulated that these failures occurring primarily from steep glaciated scarps on east and southeast aspects of the Main Divide, reflect the relatively quiescent seismic activity of the central Southern Alps during the past 100 years. Earlier and prehistoric failures from similar slopes may have occurred, but, if so, the evidence has not survived. The pre-1950 record is instead biased by typically larger (see Fig. 4) potentially earthquake-generated events (e.g. Whitehouse and Griffiths 1983; Bull and Brandon 1998; Orwin 1998; Smith et al. 2006; Chevalier et al. 2009) that may, in many instances, exhibit failure along planes of weakness, with prevalent regional bedding and schistosity dip-direction towards the west/northwest or east/southeast (Cox and Barrell 2007). The fact that modal hillslope angles do not differ significantly between western and axial domains of the Alps (Fig. 7) suggests that typically smaller magnitude post-1949 rock avalanche activity predominating from within the axial domain probably represents a geomorphologically minor process superposition within this rapidly eroding landscape. A close correspondence between general hillslope angles in eastern and axial domains of the central Southern Alps, and slopes measured within pre-1950 rock avalanche source areas attests to the importance of these typically larger, catastrophic rock avalanches forming the topography of this region. Other landslides included in this inventory encompass a range of failure types and slope lithologies (Fig. 5), with the largest failures most likely responsible for slope reduction that is particularly evident in schist bedrock of the western domain.

Rock avalanches recorded over the past century within the central Southern Alps, including those described for the Mueller Glacier, have clearly been most frequent from east–southeast facing slopes (Fig. 9, Table 3), where rocks exposed in the hangingwall of the Main Divide Fault Zone are more pervasively fractured, faulted and deformed than the greywacke of the lower

elevation footwall rocks (Cox and Findlay 1995). McSaveney (2002) previously suggested that glacier thinning has led to stress adjustment within some exceptionally steep slopes about the Main Divide, and analyses presented here have indicated that a significantly higher proportion of post-1949 rock avalanche source areas have been located in close proximity to glacial ice, compared with other bedrock slopes about the Main Divide (Fig. 11a). While necessary terrain data is currently lacking to assess surface geometric changes of small, steep ice masses, a notable decrease in ice extent has been recognised within some steep bedrock failure zones above the Mueller Glacier (Fig. 12) and may have contributed to altered stress and physical weathering regimes in these instances. Other large rockfalls catalogued from above the Murchison and Hooker Glaciers have clearly detached from steep valley flanks exposed as glaciers have thinned from their LIA limits (Table 3). Despite the remote location of glaciated slopes in the central Southern Alps, far-reaching consequences from possible rock impacts into expanding glacial lakes (Allen et al. 2009) or damming of narrow river valleys are possible.

Several recent rock avalanches have been identified as detaching from slopes that are positioned near the lower elevation limit of discontinuous permafrost, where thawing is most likely (Fig. 9 and 11b). Confirming whether or not these slopes contain thawing ice, and identifying how subsurface hydrology and thermal regimes respond to warming over seasonal to inter-annual scales will require geophysical monitoring (e.g. Krautblatter and Hauck 2007; Krautblatter et al. 2010). For example, heat advection from rainfall and snow-melt percolation may promote rapid near-surface heat fluxes in the active layer of the permafrost, superimposed on a more gradual thermal response and thickening of this layer. Determining the extent to which longer-term climate change may have influenced recent slope failure requires demonstrated evidence that the landslide distribution has notably changed over time. For a given period of warming, approaches exist to simulate changes in bedrock temperature with depth and variations in marginal permafrost limits within complex terrain (Noetzli and Gruber 2009); changes which should theoretically correspond with zones of increased instability over time. However, large-magnitude, high-elevation failures are known to be missing from the inventory used in this study. For example, a large pre-1900 rock avalanche was reported to have originated near the summit of Aoraki/Mt. Cook (Barff 1873), but no further details or evidence are known. Distinct avalanche lobes visible on the lower Hooker Glacier in photographs from 1893 are located too far down the glacier to realistically correspond to this event and therefore constitute another sequence of slope failures without a known source location (Fig. 13). Given a demonstrated loss of physical evidence from the landslide record, the necessary basis does not exist from which to quantitatively determine whether or not climate has changed the distribution and/or frequency of recent slope failure in the central Southern Alps.

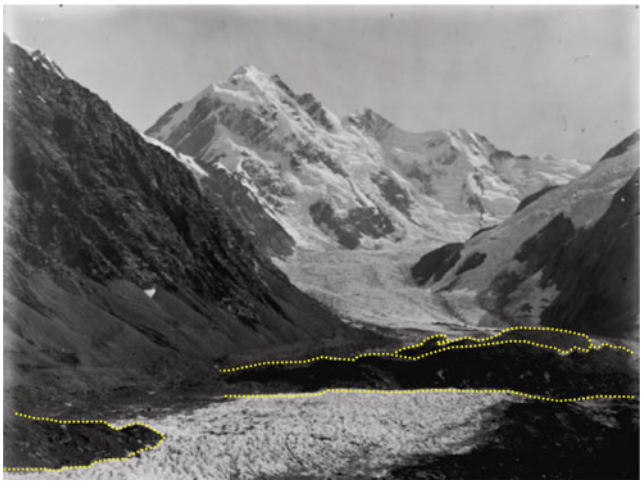

**Fig. 13** Image of the lower Hooker Glacier from 1893, viewed towards the 3,078 m high peak of La Perouse. Rock avalanche deposits are visible on the ice in the foreground, but they have left no recognised surviving geomorphic evidence (photo from the Burton brother's collection, Te Papa)

## Conclusions

Five hundred nine landslides have been analysed within a GIS inventory, with combined source and deposit areas affecting ~2% of the central Southern Alps. The pre-1950 record of landsliding in this region is demonstrably incomplete and probably significantly influenced by co-seismic failures and erosional censoring. Rock avalanching appears to be most abundant from greywacke and cleaved greywacke slopes which outcrop steeply along and east of the Main Divide. Within the schist and semischist bedrock which is exposed closer towards the Alpine Fault, other landslide types appear to predominate, and evidence for large rock avalanches is apparently less abundant west of the Main Divide. Pre-1950 rock avalanches and other landslides have prevailed from slope facing west–northwest, and the likelihood of rock avalanche failure increases on bedrock slopes exceeding 50°. Above 2,500 m in the Alpine zone, rock avalanching appears to be the primary large magnitude mechanism for bedrock-slope failure, and post-1949, many apparently spontaneous events have been recorded, occurring most frequently from east–southeast aspects on the hanging-wall of the Main Divide Fault Zone. It has been demonstrated that the occurrence of these recent failures is significantly greater from bedrock slopes located in close proximity to glaciers, where ice retreat may have been a relevant factor. Similarly, a higher proportion of post-1949 detachment surfaces are observed within 300 m of the lower limit of permafrost occurrence, where thawing of ice bonded bedrock is possible. However, demonstrating any influence of atmospheric warming, permafrost degradation and perennial ice melt on recent higher elevation slope failures and more importantly, distinguishing these influences from tectonic and other climatic forcing is not yet possible. Irrespective of any direct role climate variability might have had, or could have, the occurrence of numerous recent failures from steep, fractured greywacke slopes of the central Southern Alps, implies that the next major earthquake in the region will trigger many more failures from these same slopes, and some of these may be very large.

## Acknowledgements

This project was supported by a University of Canterbury doctoral scholarship, with additional project funding provided by the New Zealand Earthquake Commission. David Barrell is thanked for his contributions mapping landslides in the region,

helping to build the GIS dataset and providing thoughtful discussions on various aspects of this research. We are grateful for many positive suggestions given by Christian Huggel. In addition, comprehensive reviews and many constructive suggestions were provided by Tim Davies (editor), Oliver Korup, Wilfried Haeberli and an anonymous third reviewer.

## References

Adams J (1981) Earthquake dammed lakes in New Zealand. Geology 9:215–219

Allen S, Owens I, Sirguey P (2008a) Satellite remote sensing procedures for glacial terrain analyses and hazard assessment in the Aoraki Mount Cook region, New Zealand. NZ J Geol Geophys 51:73–87

Allen S, Owens I, Huggel C (2008b) A first estimate of mountain permafrost distribution in the Mount Cook region of New Zealand's Southern Alps. In: Kane DL, Hinkel KM (eds) Ninth International Conference on Permafrost, Institute of Northern Engineering. University of Alaska, Fairbanks, pp 37–42

Allen SK, Schneider D, Owens IF (2009) First approaches towards modelling glacial hazards in the Mount Cook region of New Zealand's Southern Alps. Nat Hazards Earth Syst Sci 9:481–499

Ballantyne CK (2002) Paraglacial geomorphology. Quatern Sci Rev 21:1935–2017

Barff E (1873) A letter respecting the recent change in the apex of Mount Cook communicated by J. Hector. Trans Proc N Z Inst 6:379–380

Barringer JRF, McNeill SJ, Pairman D (2002) Progress on assessing the accuracy of a high-resolution digital elevation model for New Zealand. In: Hunter G, Lowell K (eds) 5th International Symposium on Spatial Accuracy Assessment in Natural Resources and Environmental Sciences, July 10–12. Melbourne, Australia

Bishop DG, Hislop WF (1983) Things that go bang in the night. Landscape 13:2–5

Blair RW Jr (1994) Moraine and valley wall collapse due to rapid deglaciation in Mount Cook National Park, New Zealand. Mt Res Dev 14(4):347–358

Bottino G, Chiarle M, Joly A, Mortara G (2002) Modelling rock avalanches and their relation to permafrost degradation in glacial environments. Permafrost Periglac Process 13:283–288

Brazier V, Kirkbride MP, Owens IF (1998) The relationship between climate and rock glacier distribution in the Ben Ohau Range, New Zealand. Geogr Ann 80 A(3-4):193–207

Bull WB, Brandon MT (1998) Lichen dating of earthquake-generated regional rockfall events, Southern Alps, New Zealand. Geol Soc Am Bull 110(1):60–84

Chevalier G, Davies TR, McSaveney M (2009) The prehistoric Mt Wilberg rock avalanche, Westland, New Zealand. Landslides 6(4):253–262

Chinn TJH (1995) Glacier fluctuations in the Southern Alps of New Zealand determined by snowline elevations. Arct Alpine Res 27(2):187–198

Chinn T, Winkler S, Salinger MJ, Haakensen H (2005) Recent glacier advances in Norway and New Zealand: A comparison of their glaciological and meteorological causes. Geogr Ann 87 A(1):141–157

Cox SC, Allen SK (2009) Vampire rock avalanches of January 2008 and 2003, Southern Alps, New Zealand. Landslides 6:161–166

Cox S, Barrell DJA (2007) Geology of the Aoraki Area, New Zealand. Institute of Geological and Nuclear Sciences 1:250,000 geological map 15. GNS Science, Lower Hutt, New Zealand

Cox SC, Findlay RH (1995) The main divide fault zone and its role in formation of the Southern Alps, New Zealand. NZ J Geol Geophys 38:489–499

Cox SC, Sutherland R (2007) Regional geological framework of South Island, New Zealand, and its significance for understanding the active plate boundary. In: Okaya DA, Stern TA, Davey FJ (eds) A continental plate boundary: tectonics at South Island, New Zealand. Geophysical Monography 175, American Geophysical Union, Washington DC, pp 19–46

Cox SC, Allen SK, Ferris BG (2008) Vampire rock avalanches, Aoraki/Mount Cook National Park. GNS Science report 2008/10, Institute of Geological and Nuclear Sciences. Lower Hutt, New Zealand

Crozier MJ, Deimel MS, Simon JS (1995) Investigation of earthquake triggering for deep-seated landslides, Taranaki, New Zealand. Quatern Int 25:65–73

Cruden DM, Varnes DJ (1996) Landslide types and processes. In: Turner AK, Schuster RL (eds) Landslides—investigation and mitigation. Transportation Research Board, Washington, pp 36–75

Davies MCR, Hamza O, Harris C (2001) The effect of rise in mean annual temperature on the stability of rock slopes containing ice-filled discontinuities. Permafrost Periglac Process 12(1):69–77

Deline P (2009) Interactions between rock avalanches and glaciers in the Mont Blanc massif during the late Holocene. Quatern Sci Rev 28(11–12):1070–1083

Densmore AL, Hovius N (2000) Topographic fingerprint of bedrock landslides. Geology 28:371–374

Donati L, Turrini MC (2002) An objective method to rank the importance of the factors predisposing to landslides with the GIS methodology: application to an area of the Apennines (Valnerina; Perugia, Italy). Eng Geol 63:277–289

Dramis F, Govi M, Guglielmin M, Mortara G (1995) Mountain permafrost and slope instability in the Italian Alps: The Val Pola Landslide. Permafrost Periglac Process 6:73–82

Evans SG, Clague JJ (1988) Catastrophic rock avalanches in glacial environment. Proceedings of the 5th International Symposium on Landslides 2:1153–1158

Fischer L, Kääb A, Huggel C, Noetzli J (2006) Geology, glacier retreat and permafrost degradation as controlling factors of slope instabilities in a high-mountain rock wall: the Monte Rosa east face. Nat Hazards Earth SystSci 6:761–772

Fitzsimons SJ (1997) Late-glacial and early holocene glacier activity in the Southern Alps, New Zealand. Quatern Int 38(39):69–76

Fitzsimons SJ, Veit H (2001) Geology and geomorphology of the European Alps and the Southern Alps of New Zealand. Mt Res Dev 21(4):340–349

Geertsema M, Clague JJ, Schwab JW, Evans SG (2006) An overview of recent large catastrophic landslides in northern British Columbia, Canada. Eng Geol 83:120–143

Griffiths GA, McSaveney MJ (1983) Distribution of mean annual precipitation across some steepland regions of New Zealand. NZ J Sci 26:197–209

Gruber S, Haeberli W (2007) Permafrost in steep bedrock slopes and its temperature-related destabilization following climate change. J Geophys Res 112. doi:10.1029/2006JF000547

Gruber S, Hoelzle M, Haeberli W (2004) Permafrost thaw and destabilization of Alpine rock walls in the hot summer of 2003. Geophys Res Lett 31(L13504)

Haeberli W (1975) Untersuchungen zur Verbreitung von Permafrost zwischen Fluelapass und Piz Grialetsch (Graubünden). Mitteilungen der Versuchsanstalt für Wasserbau, Hydrologie und Glaziologie der ETH, Zurich, 17, 221pp

Haeberli W, Wegmann M, Vonder Mühll D (1997) Slope stability problems related to glacier shrinkage and permafrost degradation in the Alps. Eclogae Geol Helv 90:407–414

Haeberli W, Huggel C, Kääb A, Zgraggen-Oswald S, Polkvoj A, Galushkin I, Zotikov I, Osokin N (2004) The Kolka-Karmadon rock/ice slide of 20 September 2002—an extraordinary event of historical dimensions in North Ossetia (Russian Caucasus). J Glaciol 50(171):533–546

Hancox GT, Cox SC, Turnbull IM, Crozier MJ (2003) Reconnaissance studies of landslides and other ground damage caused by the Mw 7.2 Fiordland earthquake of 22 August 2003. Institute of Geological and Nuclear Sciences, Science Report 2003/30, Lower Hutt

Hancox GT, McSaveney MJ, Manville VR, Davies TR (2005) The October 1999 Mt Adams rock avalanche and subsequent landslide dam-break flood and effects in Poerua River, Westland, New Zealand. NZ J Geol Geophys 48(4):683–705

Harris C (2005) Climate change, mountain permafrost degradation and geotechnical hazard. In: Huber UM, Bugmann HKM, Reasoner MA (eds) Global change and mountain regions. An overview of current knowledge. Springer, Dordrecht, pp 215–224

Harris C, Vonder Mühll D (2001) Permafrost and climate in Europe: climate change, mountain permafrost degradation and geotechnical hazard. In: Visconti G, Beniston M, Iannorelli EE, Barba D (eds) Global change in protected areas. Kluwer, Dordrecht, pp 71–72

Harris C, Vonder Mühll D, Isaksen K, Haeberli W, Sollid JL, King L, Holmlund P, Dramis F, Guglielmin M, Palacios D (2003) Warming permafrost in European mountains. Glob Planet Change 39:215–225

Hermanns RL, Strecker MR (1999) Structural and lithological controls on large Quaternary rock avalanches (sturzstroms) in arid northwestern Argentina. Geol Soc Am Bull 111(6):934–948

Hewitt K, Clague JJ, Orwin JF (2008) Legacies of catastrophic rock slope failures in mountain landscapes. Earth Sci Rev 87:1–38

Hoelzle M, Chinn T, Stumm D, Paul F, Zemp M, Haeberli W (2007) The application of glacier inventory data for estimating past climate change effects on mountain glaciers: a comparison between the European Alps and the Southern Alps of New Zealand. Glob Planet Change 56:69–82

Hovius N, Stark CP, Allen PA (1997) Sediment flux from a mountain belt derived from landslide mapping. Geology 25:231–234

Huggel C (2009) Recent extreme slope failures in glacial environments: effects of thermal perturbation. Quatern Sci Rev 28(11–12):1119–1130

Huggel C, Salzmann N, Allen S, Caplan-Auerbach J, Fischer L, Haeberli W, Larsen C, Schneider D, Wessels R (2010) Recent and future warm extreme events and high-mountain slope failures. Philos Trans R Soc A 368:2435–2459

Hungr O, Evans SG, Bovis MJ, Hutchinson JN (2001) A review of the classification of landslides of the flow type. Environ Eng Geosci VII(3):221–238
Kääb A, Reynolds JM, Haeberli W (2005) Glacier and permafrost hazards in high mountains. In: Huber UM, Bugmann HKM, Reasoner MA (eds) Global change and mountain regions. An overview of current knowledge. Springer, Dordrecht, pp 225–234
Korup O (2002) Recent research on landslide dams—a literature review with special attention to New Zealand. Prog Phys Geogr 26(2):206–235
Korup O (2004) Geomorphic implications of fault zone weakening: slope instability along the Alpine Fault, South Westland to Fiordland. NZ J Geol Geophys 47:257–267
Korup O (2005a) Large landslides and their effect on sediment flux in South Westland. N Z Earth Surf Processes Landf 30:305–323
Korup O (2005b) Distribution of landslides in southwest New Zealand. Landslides 2:43–45
Korup O, McSaveney MJ, Davies TRH (2004) Sediment generation and delivery from large historic landslides in the Southern Alps, New Zealand. Geomorphology 61:189–207
Korup O, Schmidt J, McSaveney M (2005) Regional relief characteristics and denudation pattern of the western Southern Alps, New Zealand. Geomorphology 71:402–423
Krautblatter M, Hauck C (2007) Electrical resistivity tomography monitoring of permafrost in solid rock walls. J Geophys Res 112. doi:10.1029/2006JF000546)
Krautblatter M, Verleysdonk S, Flores-Orozco A, Kemna A (2010) Temperature-calibrated imaging of seasonal changes in permafrost rock walls by quantitative electrical resistivity tomography (Zugspitze, German/Austrian Alps). J Geophys Res 115. doi:10.1029/2008JF001209
Larsen SH, Davies TR, McSaveney MJ (2005) A possible coseismic landslide origin of Late Holocene moraines of the Southern Alps, New Zealand: short communication. NZ J Geol Geophys 48(2):311–314
Lillie AR, Gunn BM (1964) Steeply plunging folds in the Sealy Range. NZ J Geol Geophys 7:404–423
McSaveney MJ (2002) Recent rockfalls and rock avalanches in Mount Cook National Park, New Zealand. Geol Soc Am Rev Eng Geol XV:35–69
Nadim F, Kjekstad O, Peduzzi P, Herold C, Jaedicke C (2006) Global landslide and avalanche hotspots. Landslides 3:159–173
Newham RM, Lowe DJ, Williams PW (1999) Quaternary environmental change in New Zealand: a review. Prog Phys Geogr 23(4):567–610
Norris RJ, Cooper AF (2001) Late Quaternary slip rates and slip partitioning on the Alpine Fault. N Z J Struct Geol 23:507–520
Noetzli J, Gruber S (2009) Transient thermal effect in Alpine permafrost. The Cryosphere 3:85–99
Noetzli J, Hoelzle M, Haeberli W (2003) Mountain permafrost and recent Alpine rock-fall events: a GIS-based approach to determine critical factors. In: Phillips M, Springman SM, Arenson LU (eds) PERMAFROST, Proceedings of the Eighth International Conference on Permafrost. Swets and Zeitlinger, Zurich, Switzerland, pp 827–832
Orwin JF (1998) The application and implications of rock weathering-rind dating to a large rock avalanche, Craigieburn Range, Canterbury, New Zealand. NZ J Geol Geophys 41:219–223
Pande A, Joshi RC, Jalal DS (2002) Selected landslide types in the Central Himalaya: their relation to geological structure and anthropogenic activities. Environmentalist 22 (3):269–287
Paterson BR (1996) Slope instability along state highway 73 through Arthur's Pass, South Island, New Zealand. NZ J Geol Geophys 39:339–351
Pearce AJ, O'Loughlin CC (1985) Landsliding during a M7.7 earthquake: influence of geology and topography. Geology 13:855–858
Pike RJ, Graymer RW, Sobieszczyk S (2003) A simple GIS model for mapping landslide susceptibility. In: Evans IS, Dikau R, Tokunaga E, Ohmori H, Hirano M (eds) Concepts and modelling in geomorphology: international perspectives. TERRAPUB, Tokyo
Rattenbury MS, Heron DW, Nathan S (1994) Procedures and specifications for the QMAP GIS. GNS Science report 94/42, Institute of Geological and Nuclear Sciences, Lower Hutt, New Zealand
Salinger JM, Basher RE, Fitzharris B, Hay JE, Jones PD, MacVeigh JP, Schmidely-Leleu I (1995) Climate trends in the South-West Pacific. Int J Climatol 15:285–302
Shulmeister J, Davies TR, Evans DJA, Hyatt OM, Tovar DS (2009) Catastrophic landslides, glacier behaviour and moraine formation—a view from an active plate margin. Quatern Sci Rev 28(11–12):1085–1096
Smith GM, Davies TR, McSaveney MJ, Bell DH (2006) The Acheron rock avalanche, Canterbury, New Zealand—morphology and dynamics. Landslides 3:62–72
Speight R (1933) The Arthur's Pass earthquake of 9 March 1929. N Z J Sci Technol 15:173–182
Suggate RP, Wilson DD (1958) Geology of the Harper and Avoca valleys, mid-Canterbury, New Zealand. NZ J Geol Geophys 1:31–46
Sutherland R, Eberhart-Phillips D, Harris RA, Stern TA, Beavan RJ, Ellis SM, Henrys SA, Cox SC, Norris RJ, Berryman KR, Townend J, Bannister SC, Pettinga J, Leitner B, Wallace LM, Little TA, Cooper AF, Yetton M, Stirling MW (2007) Do great earthquakes occur on the Alpine Fault in central South Island, New Zealand? In: Okaya DA, Stern TA, Davey FJ (eds) A continental plate boundary: tectonics at South Island, New Zealand. Geophysical Monography 175, American Geophysical Union, Washington, DC, pp 235–251
Turnbull JM, Davies TRH (2006) A mass movement origin for cirques. Earth Surf Process Land 31:1129–1148
Wegmann M, Gudmundsson GH, Haeberli W (1998) Permafrost changes in rock walls and the retreat of Alpine glaciers: a thermal modelling approach. Permafrost Periglac Process 9:23–33
Wells A, Duncan RP, Stewart GH, Yetton MD (1999) Prehistoric dates of the most recent Alpine Fault earthquakes, New Zealand. Geology 27:995–998
Whitehouse IE (1983) Distribution of large rock avalanche deposits in the central Southern Alps, New Zealand. NZ J Geol Geophys 26:272–279
Whitehouse IE (1988) Geomorphology of the central Southern Alps, New Zealand: the interaction of plate collision and atmospheric circulation. Z Geomorphol 69:105–116
Whitehouse IE, Griffiths GA (1983) Frequency and hazard of large rock avalanches in the central Southern Alps, New Zealand. Geology 11:331–334

**S. Allen · I. Owens**
Department of Geography,
University of Canterbury,
Christchurch, New Zealand

**S. Allen (✉)**
Climate and Environmental Physics, Physics Institute,
University of Bern,
Bern, Switzerland
e-mail: simon.allen@phil.unibe.ch

**S. Cox**
GNS Science,
Private Bag 1930,
Dunedin, New Zealand